

# Gaussian RBFNet: Gaussian Radial Basis Functions for Fast and Accurate Representation and Reconstruction of Neural Fields

Abdelaziz Bouzidi, Hamid Laga, Hazem Wannous

**Abstract**—Neural fields such as DeepSDF and Neural Radiance Fields have recently revolutionized novel-view synthesis and 3D reconstruction from RGB images and videos. However, achieving high-quality representation, reconstruction, and rendering requires deep neural networks, which are slow to train and evaluate. Although several acceleration techniques have been proposed, they often trade off speed for memory. Gaussian splatting-based methods, on the other hand, accelerate the rendering time but remain costly in terms of training speed and memory needed to store the parameters of a large number of Gaussians. In this paper, we introduce a novel neural representation that is fast, both at training and inference times, and lightweight. Our key observation is that the neurons used in traditional MLPs perform simple computations (a dot product followed by ReLU activation) and thus one needs to use either wide and deep MLPs or high-resolution and high-dimensional feature grids to parameterize complex nonlinear functions. We show in this paper that by replacing traditional neurons with Radial Basis Function (RBF) kernels, one can achieve highly accurate representation of 2D (RGB images), 3D (geometry), and 5D (radiance fields) signals with just a single layer of such neurons. The representation is highly parallelizable, operates on low-resolution feature grids, and is compact and memory-efficient. We demonstrate that the proposed novel representation can be trained for 3D geometry representation in less than 15 seconds and for novel view synthesis in less than 15 mins. At runtime, it can synthesize novel views at more than 60 fps without sacrificing quality. Our code is available at <https://grbfnet.github.io/>.

**Index Terms**—Radial Basis Functions, Neural Radiance Fields, Deep SDF, 3D reconstruction, novel view synthesis, neural rendering.



## 1 INTRODUCTION

IN recent years, neural fields have gained in popularity for their ability to accurately represent multidimensional signals such as RGB images and videos [1], [2], 3D geometry [3], [4], and radiance fields [4], [5]. Compared to traditional discrete signal representations, neural fields use Multi-Layer Perceptrons (MLP) to learn a mapping from a continuous input, *e.g.*, a 2D point  $p \in \mathbb{R}^2$ , a 3D point  $p \in \mathbb{R}^3$ , or a 3D point and a viewing direction  $\mathbf{v} \in \mathbb{S}^2$ , to the corresponding output value such as RGB color, SDF value or volume density, and radiance. This efficient formulation has achieved state-of-the-art results in applications such as 3D reconstruction, neural rendering and novel view synthesis, virtual (human and animal) avatar reconstruction and generation, and many more.

Despite their performance, neural fields are very slow to train (*e.g.*, traditional NeRF can take hours to train on a single scene) and evaluate, and are expensive in terms of memory requirements. Although several acceleration techniques have been proposed, they either focus on accelerating the inference stage [6], [7], [8] or trade speed for memory [7], [9]. For instance, methods such as Plenoxels [7]

and InstantNGP [9] achieve fast training but result in a significant memory footprint for storing the feature grids and network parameters. On the other hand, 3D Gaussian Splatting (3DGS)-based methods [10], which are explicit representations, achieve realtime rendering performance by parameterizing the radiance field using 3D Gaussians instead of MLPs. These methods, however, require a large number of Gaussians to accurately represent 3D scenes, which makes them expensive in terms of memory requirements. Also, although they are very fast at runtime, they can still require hours to train per scene.

In this work, we propose a novel neural representation that is compact, memory-efficient, and fast to train and evaluate without sacrificing quality or memory. Our key observation is that the neurons used in MLP-based neural fields perform simple computations: a dot product followed by an activation function, usually ReLU. Thus, to parameterize complex functions, one needs to stack multiple layers of such neurons, leading to wide and deep MLPs that have a large number of parameters. Thus, they are difficult and time-consuming to train and evaluate. In this paper, we show that by letting the neurons perform slightly more than just a dot product, we can significantly reduce the depth and width of the network used in neural field representations. In particular, we propose a novel architecture composed of a single layer of a small number of Radial Basis Function kernels that decode a low-resolution feature grid. We show that this compact representation is sufficient to accurately represent multidimensional signals such as RGB images, 3D geometry, and radiance fields. More importantly, it can

- Abdelaziz Bouzidi is with the School of Information Technology, Murdoch University (Australia) and with IMT Nord Europe (France). Email: [abdelaziz.bouzidi@murdoch.edu.au](mailto:abdelaziz.bouzidi@murdoch.edu.au).
- Hamid Laga is with the School of Information Technology, Murdoch University (Australia). Email: [H.Laga@murdoch.edu.au](mailto:H.Laga@murdoch.edu.au)
- Hazem Wannous is with IMT Nord Europe (France). Email: [hazem.wannous@imt-nord-europe.fr](mailto:hazem.wannous@imt-nord-europe.fr).

Manuscript received Marc. 8, 2025.

be trained, on a desktop PC equipped with an NVIDIA GEFORCE RTX4090 GPU, in less than 15 secs for 3D geometry representation and in less than 15 mins for novel view synthesis. At runtime, it can render novel views at more than 60 fps without sacrificing quality.

The remaining parts of the paper are organized as follows; Section 2 reviews the state-of-the-art. Sections 3, 4, 5, and 6 describe in detail the proposed framework. Sections 7 presents the results and analyzes the performance of the proposed framework. Section 8 summarizes the main findings of the paper and discusses its limitations and avenues for future research.

## 2 RELATED WORK

We refer the reader to recent comprehensive surveys of the state-of-the-art on neural fields [11] and 3D Gaussian Splatting [12]. Here, we focus on the papers that are closely related to our work.

### Neural fields

Neural fields use MLPs to represent signals such as 2D images [9], [13], [14], SDF values [3], [4], [15], [16], and radiance fields [5] as continuous functions. While powerful, these methods require querying deep and wide MLPs – often composed of dozens of layers and thousands of neurons – millions of times, both during training and at runtime. As such, training scene-specific neural fields can take hours or days for each scene.

Several methods have been proposed to accelerate the training and inference of neural fields. In particular, feature grid-based neural fields [9] significantly improve inference time by shifting most of the computation burden to the features and then using shallow MLPs to decode them into geometry and appearance. However, they are very expensive in terms of memory requirement, as the space required to store the features exceeds that of the network parameters. Some methods improve the computation time by reducing the number of forward passes through early ray termination [17], [18] or efficient surface localization [6], [7], [17], [18], [19], [20], [21], [22], [23]. Others employ baking strategies by precomputing and storing some content in sparse 3D data structures [24], [25], [26], [27]. PlenOctrees [23], on the other hand, represent view-dependent effects as a weighted sum of Spherical Harmonic (SH) basis, parameterized by the viewing direction. The view-dependent color can then be computed in a single forward pass. Plenoxels [23] follows the same idea but drops entirely the MLPs and represents a scene as a sparse 3D grid with spherical harmonics. The representation can be optimized without any neural components.

While these acceleration techniques can reduce training time to less than 10 mins [7], [9], they remain very expensive in terms of memory requirements.

### Point-based differentiable radiance fields

3D Gaussian Splatting (3DGS) [10] achieves realtime rendering of high-resolution images without relying on deep neural networks. The idea is to represent a scene’s geometry and radiance field with a large number of 3D Gaussians whose parameters are learnable. Although 3DGS achieves

impressive rendering performance, it can be slow at training and is memory-consuming since it needs to store a large number of Gaussians, usually in the order of millions. Subsequent works reduce the memory requirements of 3DGS-based methods, and thus improve their scalability, by pruning insignificant Gaussians [28], [29], [30] or compressing the memory usage of 3D Gaussian properties [28], [29], [31]. Although these methods achieve compression ratios of several to dozens of times for storage after training, there remains considerable potential for reducing memory usage during the training phase.

### Radial Basis Functions

Carr *et al.* [32] showed that the SDF of complex 3D objects can be accurately represented using Radial Basis Functions (RBFs). RBFs can be interpreted as a neural network, termed RBF network, that has an input layer and one output neuron. However, unlike traditional MLPs, a neuron in the input layer performs a slightly more complex transformation of its input by using a kernel function, referred to as a basis function, such as a Gaussian or a thin-plate spline. To accurately represent complex 3D geometries, Carr *et al.* [32] use a large number of basis functions, in the order of 80K. To optimize the representation and speed up training and inference, Kojekine *et al.* [33] use RBFs with compact support. Ohtake *et al.* [34] use a hierarchical space-partitioning structure that accelerates training and allows to select the basis function type that best fits the local geometry.

In the era of deep learning, only a few papers have explored the use of RBF kernels in representing neural fields. For instance, Ramasinghe *et al.* [35], [36] proposed a broader class of activation functions, including Gaussians, that enable coordinate MLPs to encode high-frequency signals. They demonstrated that coordinate-based Gaussian MLPs show much better convergence properties against various initialization schemes compared to sinusoid and ReLU-based activations. Chng *et al.* [37] use Gaussian MLPs for joint pose estimation and scene reconstruction. Chen *et al.* [13] use RBFs to learn the location of the local features, instead of pre-setting them on regular 3D or 2D grids, and efficiently interpolate them, instead of using trilinear interpolation. Chen *et al.* [14], [38], on the other hand, use basis functions for input encoding, instead of the commonly used frequency encoding. Different from these methods is the approach of Jian *et al.* [39], which uses a decoding MLP composed of traditional linear layers followed by one or multiple quadratic layers. Although some of these methods have demonstrated a gain in representation accuracy, they all require MLPs with a large number of layers and a large number of neurons per layer to represent signals of interest. For instance, NeuRBF [13] still requires a deep MLP to decode the interpolated feature into the output signal value. CoFie of Jian *et al.* [39] only replaces the top layer of the MLP with a quadratic layer. Although it allows a better representation of the quadratic component of the SDF function, the method still requires a network of five layers (four standard linear layers followed by ReLU activation and one quadratic layer).

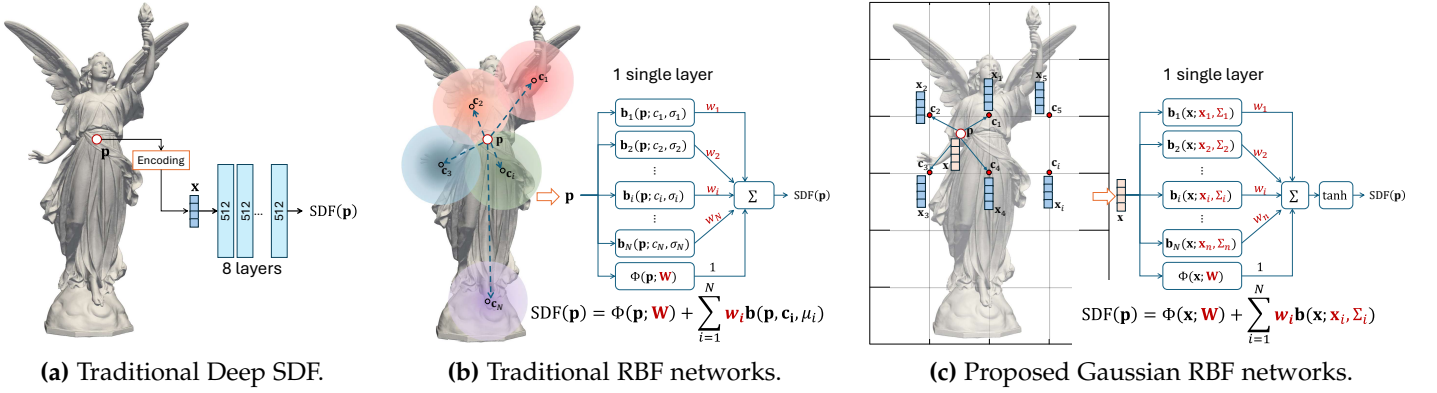


Fig. 1. Illustration of the proposed Gaussian RBFNet in comparison to the traditional neural fields such as Deep SDF and the traditional RBF networks for 3D geometry representation.

### Contributions

Compared to the state-of-the-art, our contribution is two-fold; **First**, we introduce a novel family of neural fields that use RBF kernels to decode low-resolution feature grids into high-quality nD signals. **Second**, we demonstrate that a single-layer RBF network, composed of a small number of neurons with learnable Gaussian kernels, *i.e.*, Gaussian kernels whose parameters are all learnable, is sufficient to efficiently represent RGB images, 3D geometry, and radiance fields. Extensive experiments demonstrate that our formulation has several benefits compared to the state-of-the-art: it is fast to train (less than 0.5 mins for SDF representation and around 14 mins for radiance fields representation). It can render images at more than 60 fps and is significantly compact.

## 3 NEURAL FIELDS

Neural fields (Figure 1-(a)) represent a signal  $f : \mathbb{R}^d \rightarrow \mathbb{R}^q$ , which maps a point  $p \in \mathbb{R}^d$  to a  $q$ -dimension output, with  $d \geq 1, q \geq 1$ , as a continuous function of the form  $f = h \circ \gamma$  where:

- $\gamma : \mathbb{R}^d \rightarrow \mathbb{R}^m$  is an encoding function that maps a point  $p \in \mathbb{R}^d$  to a neural feature  $\mathbf{x} \in \mathbb{R}^m$ , and
- $h : \mathbb{R}^m \rightarrow \mathbb{R}^q$  is a decoding function that extracts the desired output from the neural feature  $\mathbf{x} = \gamma(p) \in \mathbb{R}^m$ .

Point encoding-based neural fields define  $\gamma$  as a multi-frequency sinusoid function. Explicit neural fields use features organized into grids. The encoding  $\gamma(p)$  of a point  $p \in \mathbb{R}^d$  is then determined by trilinearly interpolating the grid features that are around the point.

Different from these methods is NeuRBF [13], which, instead of using trilinear interpolation, it uses Radial Basis Functions (RBFs) as an interpolant to compute the feature at  $p$ . Furthermore, instead of predefining the location of the features (as the corners of a regular grid in  $\mathbb{R}^3$ ), NeuRBF [13] defines these locations as the centers of the Radial Basis Functions. Both the centers, the shape, and the blending weights are learnable parameters that are optimized during training.

To parameterize the function  $h$ , which decodes the learned feature into the target output, state-of-the-art methods, including NeuRBF [13], use deep MLPs composed of multiple layers, each one is followed by an activation function, usually ReLU. In this paper, we revisit this decoding function and demonstrate that a single layer composed of a small number of RBF kernels (or nodes) is sufficient to achieve state-of-the-art performance. Thus, our method is orthogonal and complementary to existing methods.

### 3.1 Radial Basis Functions

Consider a 1D signal of the form  $f : \Omega \subseteq \mathbb{R}^3 \rightarrow \mathbb{R}$ . A commonly used approach is to represent the value of the signal  $f$  at  $p \in \Omega$  as a weighted sum of basis functions:

$$\forall p \in \Omega, f(p) = \Phi(p) + \sum_{i=1}^N w_i \mathbf{b}_i(p; \Theta_i), \quad (1)$$

where  $\{\mathbf{b}_i\}_{i=1}^N$  are real-valued basis functions defined on  $p \in \Omega$  and parameterized by  $\Theta_i$ ,  $w_i \in \mathbb{R}$  are blending weights, and  $\Phi$  is a polynomial of low degree. Commonly used basis functions include Fourier bases, Wavelet functions, and Radial Basis Functions (RBFs). In this paper, we are interested in RBFs of the form:

$$f(p) = \Phi(p) + \sum_{i=1}^N w_i \mathbf{b}_i(\|p - c_i\|; \Theta_i), \quad (2)$$

which have been used to represent signed distance functions [32]. Here,  $\mathbf{b}_i : \mathbb{R}_{\geq 0} \rightarrow \mathbb{R}$  is a real-valued basis function on  $\mathbb{R}_{\geq 0} = [0, \infty)$ , centered at a point  $c_i \in \Omega$  and has  $\Theta_i$  as additional parameters. Popular choices for  $\mathbf{b}$  include the thin-plate spline and the Gaussian function. In the latter case,  $\mathbf{b}(r) = \exp(-ar^2)$  where the parameter  $a$  is the inverse of the variance and controls the shape of the Gaussian.

As shown in Figure 1-(b), an RBF function can be implemented as a feedforward network composed of (1) an input layer with  $N + 1$  neurons. The  $i$ -th neuron applies the  $i$ -th basis function  $\mathbf{b}_i$  to its input while the  $(N + 1)$ -th neuron implements the polynomial  $\Phi$ , and (2) an output layer composed of a single neuron that computes the weighted sum of the outputs of the neurons in the previous layer. It can also be considered as a neural field where the encoding function  $\gamma$  is set to identity and thus  $f = h$ . During

training, the centers  $c_i$  of the basis functions are preset in advance, usually selected to be on and around the signal of interest, while the blending weights  $w_i$  are learnable. This formulation is not new. For example, using Gaussian basis functions leads to what is commonly known as RBF networks. Also, Carr *et al.* [32] demonstrated that thin-plate spline-based RBFs can be used to represent the SDF of 3D objects. However, representing complex 3D objects requires a large number of basis functions, in the order of  $N \geq 80K$ .

### 3.2 RBF Nets for neural fields representation

Equations (1) and (2) consider 1D signals with  $d = 3$  and the output dimension is  $q = 1$ . However, neural fields are multidimensional signals with  $d \geq 1$  and  $q \geq 1$ , *e.g.*, ( $d = 3, q = 1$ ) for signed distance fields, ( $d = 2, q = 3$ ) in the case of RGB images, and ( $d = 5, q = 4$ ) in the case of radiance fields. Also, the input signal, when encoded using the encoding function  $\gamma$ , results in a high-dimensional feature. Thus, we propose to parameterize the decoding function  $h$  using Radial Basis Functions by generalizing this formulation to arbitrary-dimensional signals. Let  $\mathbf{x} = \gamma(p) \in \mathbb{R}^m$ . Then, we define:

$$h(\mathbf{x}) = \Phi(\mathbf{x}) + \mathbf{W}^\top \mathbf{B}(\mathbf{x}; \Theta_i), \quad (3)$$

where  $\mathbf{B}(\mathbf{x}; \Theta) = (\mathbf{b}_1(\mathbf{x}; \Theta_1), \dots, \mathbf{b}_N(\mathbf{x}; \Theta_N))^\top$  and  $\{\mathbf{b}_i\}_{i=1}^N$  are defined in the same way as Equation (1). The weight matrix  $\mathbf{W}$  is defined as  $\mathbf{W} = (W^1 | \dots | W^q)$  such that  $W^k = (w_1^k, \dots, w_N^k)^\top$ , and  $\Theta_i$  are the learnable parameters of the  $i$ -th basis function.

Similar to the 1D case, Equation (3) can be implemented as a feedforward neural network of two layers where (1) the input layer has  $N + 1$  neurons. The  $i$ -th neuron ( $i = 1, \dots, N$ ) applies the  $i$ -th basis function  $\mathbf{b}_i$  to its input while the  $(N + 1)$ -th neuron implements the polynomial  $\Phi$ , and (2) the output layer is composed of  $q$  neurons where the  $k$ -th neuron computes the  $k$ -th dimension of the decoding function  $h$ . Optionally, one can add an activation function at the output layer to constrain the output to remain within a specified range. This is illustrated in Figure 1-(c).

In this paper, we use multivariate Gaussians. Thus,  $\Theta_i = (\bar{\mathbf{x}}_i, K_i)$  where  $\bar{\mathbf{x}}_i \in \mathbb{R}^m$  is the center of the basis function  $\mathbf{b}_i$  and  $K_i$ , of dimension  $m \times m$ , is its covariance matrix. Thus, each basis function has  $\frac{1}{2}m(m - 1) + m$  learnable parameters ( $\frac{1}{2}m(m - 1)$  for the covariance matrix  $K_i$  and  $m$  for the center  $\bar{\mathbf{x}}_i$ ), plus the blending weight  $w_i$ . We refer to this representation as Gaussian RBFNet (GRBF).

## 4 SIGNED DISTANCE FIELD REPRESENTATION

We first demonstrate that a Gaussian RBF network with feature grid-based input encoding can accurately learn and represent, in a compact manner, the SDF of complex 3D objects. We focus on bounded scenes, which, when normalized for translation and scale, fit within the volume  $\Omega = [0, 1]^3$ . This is a special case of Equation (3) where the input dimension is  $d = 3$  and the output dimension is  $q = 1$ .

**(1) Input encoding  $\gamma$ .** We consider feature grid-based encoding where trainable codes are arranged in a regular 3D grid and optimized, in an auto-decoding fashion, along with the

network parameters. In this paper, we adopt InstantNGP’s 16 level multi-level hash grid with grid resolutions ranging from 4 to 512. Each grid cell stores a 1D feature. The feature at any given point  $p \in \Omega$  is obtained by trilinearly interpolating the features at its surrounding grid corners, for each of the 16 resolutions of the grid. Thus, the final feature vector is of dimension  $m = 16$ .

Note that this encoding facilitates multi-resolution feature extraction, capturing the 3D geometry at different levels of detail. Our formulation, however, is general and supports any grid feature-based encoding of the input such as the triplane representation [40], [41].

**(2) Feature decoding using Gaussian RBFs.** Figure 1-(c) summarizes the model architecture. We use Gaussian RBFs defined on the 16D feature space. This enables a localized decoding, making it possible to capture fine geometric details with a significantly fewer number of Gaussians than traditional RBF. In fact, while traditional RBFs for 3D geometry representation [32] require more than 80K Gaussian kernels, our experiments show that, with our formulation, 26 to 128 Gaussian kernels are sufficient to accurately represent complex 3D geometries.

In our implementation, each Gaussian kernel  $\mathbf{b}_i$  has a spherical shape and thus, it is fully defined by its center  $\bar{\mathbf{x}}_i \in \mathbb{R}^m$  and bandwidth  $\beta_i \in \mathbb{R}_{>0}$ . The latter controls its area of influence in the feature space. All these parameters are learnable and thus they are optimized during training along with the blending weights  $\mathbf{W}$ .

Experimentally, we found that the polynomial term  $\Phi$  does not influence the capacity of the RBF network in representing SDF fields. Thus, we drop this term for 3D geometry representation.

**(3) Training.** We train the model end-to-end using the  $\mathcal{L}_1$  loss between the estimated SDF ( $f$ ) and the ground truth SDF ( $\text{SDF}_{\text{gt}}$ ):

$$\mathcal{L}_{\text{SDF}} = \frac{1}{n} \sum_{i=1}^n \frac{1}{|\text{SDF}_{\text{gt}}(p_i)| + \epsilon} |f(p_i) - \text{SDF}_{\text{gt}}(p_i)|. \quad (4)$$

Here,  $n$  is the total number of training points and  $\epsilon$  is a small real number, which allows scaling the loss to focus more on areas that are closer to the surface. During training, both the network weights, the RBF parameters, and the feature vectors are jointly optimized.

To efficiently train the model, we sample more training points near the surface than far from the surface. Following DeepSDF [3], 80% of the training points are sampled from the shape surface. Half of these points are slightly perturbed in random directions. The remaining 20% of the training points are randomly sampled from the normalized 3D space. We use the Adam optimizer, with gradients estimated with respect to the trainable parameters. At the start of the training, we sample  $N$  points  $\{c_i \in \mathbb{R}^3\}_{i=1}^N$  and initialize the centers  $\bar{\mathbf{x}}_i \in \mathbb{R}^m, i = 1, \dots, N$  of the RBFs as the feature vectors at these points, *i.e.*,  $\bar{\mathbf{x}}_i = \gamma(c_i)$ . The RBF centers are then optimized during training in an auto-decoding fashion.

**(4) Hierarchical modeling.** As shown in Figure 2, our formulation enables a multiscale representation of the 3D geometry, as a by-product. In particular, the first dimensions of the feature vector  $\mathbf{x}$  correspond to the coarse shape while

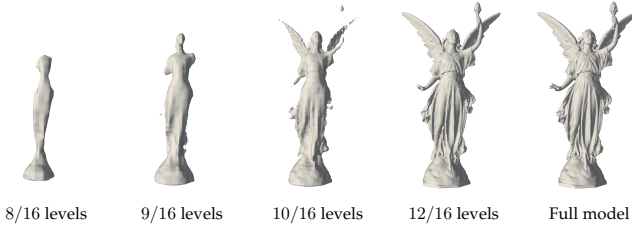


Fig. 2. Illustration of the multi-scale nature of the proposed Gaussian RBF-based representation of 3D geometry.

the latter dimensions encode high frequency geometric details. Unlike state-of-the-art feature grid representations, our formulation takes full advantage of this property because the embedding of the query points is not directly utilized by the geometry decoder. Instead, it is used to compute the Euclidean distance between the feature embeddings and the Gaussian kernel centers within the same feature space. Since the Euclidean distance is dimension-agnostic, any number of levels of the feature grid can be employed to estimate the distance of a query point to the kernel centers. Consequently, a 3D geometry can be obtained for a specific range of levels without requiring any modification to the Gaussian RBF network, enabling a multiscale representation of the output signal. Furthermore, the number of levels, considered as a hyperparameter of the feature encoding, can be adjusted to match a desired number of intermediate representations.

## 5 RGB IMAGE REPRESENTATION

Next, we focus on fitting and representing multi-dimensional signals, *i.e.*,  $d \geq 1$  and  $q \geq 1$ , using the proposed Gaussian RBF network. A typical example of such signals is RGB images, which can be seen as signals of the form  $f : [0, 1]^2 \subset \mathbb{R}^2 \times [0, 1]^3 \subset \mathbb{R}^3$  (thus,  $d = 2$  and  $q = 3$ ). They map a pixel  $p$  into its RGB color. To represent such signals, we leverage the multi-channel capability of the proposed Gaussian RBF network of Equation (3).

**(1) Input encoding  $\gamma$ .** Similar to the SDF representation, we use a hierarchical feature grid-based input encoding. We follow the same setup as of the SDF case but this time, the trainable codes are arranged in a multiresolution 2D grid. The final feature vector at a given pixel  $p \in [0, 1]^2$  is of dimension  $m = 16$ .

**(2) Feature decoding using Gaussian RBFs.** We decode the feature  $\mathbf{x} \in \mathbb{R}^m$  (with  $m = 16$ ) using a Gaussian RBF network composed of 64 Gaussian kernels and the polynomial term  $\Phi$  set to identity. Similar to the SDF case, we found that using spherical Gaussian kernels is sufficient to efficiently represent complex images.

**(3) Training.** We train the model end-to-end using the  $\mathcal{L}_2$  loss between the estimated colors  $\tilde{f}$  and the ground truth colors  $f$ :

$$\mathcal{L}_{\text{RGB}} = \frac{1}{n} \sum_{i=1}^n \left| \tilde{f}(p_i) - f(p_i) \right|^2. \quad (5)$$

Here,  $n$  is the number of training pixels. During training, both the network weights, the RBF parameters, and the feature vectors are jointly optimized. At the start of the training,

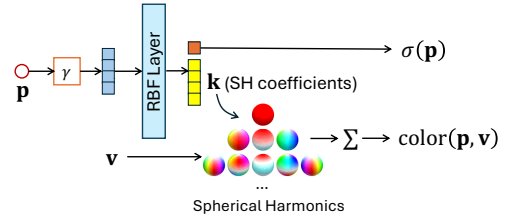


Fig. 3. Architecture of the proposed RBF-based network for radiance field representation and novel view synthesis.

we regularly sample  $N$  pixels  $\{c_1, \dots, c_N\}$  in the image space and initialize the centers  $\bar{\mathbf{x}}_i \in \mathbb{R}^m$ ,  $i = 1, \dots, N$  of the RBFs as the feature vectors at these pixels, *i.e.*,  $\bar{\mathbf{x}}_i = \gamma(c_i)$ . The RBF centers are then optimized, jointly with the other trainable parameters, in an auto-decoding fashion.

## 6 RADIANCE FIELD RECONSTRUCTION

Finally, we demonstrate how the proposed Gaussian RBF Network can be used to represent radiance fields and synthesize novel views. A radiance field is a function  $f$  of the form:

$$f : \mathbb{R}^3 \times \mathbb{S}^2 \rightarrow \mathbb{R}^4, p \in \mathbb{R}^3 \mapsto (\sigma, \mathbf{x}_{\text{geo}}) = h_{\text{geo}}(\gamma(p)), \quad (6)$$

$$\mathbf{x}_{\text{geo}}, \mathbf{v} \in \mathbb{S}^2 \mapsto c = h_{\text{color}}(\mathbf{x}_{\text{geo}}, \gamma(\mathbf{v})).$$

Here,  $\sigma$  is the volume density at  $p$ ,  $c$  is its RGB color as viewed from the viewing direction  $\mathbf{v} \in \mathbb{S}^2$ ,  $\mathbf{x}_{\text{geo}}$  is a latent code that encodes the geometry at  $p$ , and  $h_{\text{geo}}$  and  $h_{\text{color}}$  are, respectively, the geometry and color decoding functions. Note that, although  $\mathbf{v} \in \mathbb{S}^2$ , in our implementation, we represent it as a unit vector in  $\mathbb{R}^3$ .

**(1) Input encoding.** Similar to the SDF representation, we use a hierarchical feature grid-based encoding with 64 different resolutions and 1D feature per resolution. Thus, the final feature vector at a given point  $p$  is of dimension  $m = 64$ .

**(2) Network architecture.** To implement the radiance field  $f$ , we propose a fully Gaussian RBF-based representation of the decoding functions  $h_{\text{geo}}$  and  $h_{\text{color}}$ . Following PlenOctree [23], we factorize the appearance via closed-form spherical harmonic basis. We represent the view-dependent color  $h_{\text{color}}$ , which is a function of the viewing direction  $\mathbf{v}$ , as a weighted sum of spherical harmonics, *i.e.*,

$$h_{\text{color}}(\mathbf{v}, \mathbf{k}) = c(\mathbf{v}; \mathbf{k}) = \sum_{l=0}^{l_{\text{max}}} \sum_{m=-l}^l k_l^m Y_l^m(\mathbf{v}), \quad (7)$$

where  $\mathbf{k} = \{k_l^m\}_{0 \leq l \leq l_{\text{max}}, -l \leq m \leq l}$  are the spherical harmonic coefficients and  $Y_l^m : \mathbb{S}^2 \rightarrow \mathbb{R}$  are the spherical harmonic basis, which we define as functions of the viewing direction  $\mathbf{v} \in \mathbb{S}^2$ .

Next, we modify the geometry decoding function  $h_{\text{geo}}$  to output the volume density  $\sigma$  and 16 spherical harmonic coefficients per color channel; see Figure 3-(b). Thus, the number of output neurons in the geometry network is set to  $1 + 16 \times 3 = 49$ .

The main advantage of this representation is that the entire model uses only one Gaussian RBF network, which

Model	CD-L1 ( $\downarrow$ )	NC ( $\uparrow$ )	NAE ( $\downarrow$ )	IoU ( $\uparrow$ )	Tr. Time (s)	Parameters
<b>GRBFNet (Ours)</b>	<b>0.0026 <math>\pm</math> 0.0019</b>	<b>0.9429 <math>\pm</math> 0.0634</b>	<b>11.996 <math>\pm</math> 7.9340</b>	<b>0.9628 <math>\pm</math> 0.0404</b>	<b>15</b>	<b>3,840,108</b>
NeuRBF [13]	0.0057 $\pm$ 0.0060	0.8950 $\pm$ 0.1296	16.940 $\pm$ 14.727	0.9056 $\pm$ 0.1140	54	950,409
Factorfields [38]	0.0041 $\pm$ 0.0034	0.9162 $\pm$ 0.0904	15.637 $\pm$ 10.645	0.9318 $\pm$ 0.0684	20	5,342,274
InstantNGP [9]	0.0029 $\pm$ 0.0024	0.9350 $\pm$ 0.0771	12.574 $\pm$ 9.6156	0.9598 $\pm$ 0.0515	21	6,125,048

TABLE 1

We quantitatively evaluate the performance of the proposed method in reconstructing and representing Signed Distance Fields, and compare it against three state-of-the-art methods. The best values are highlighted in green and the second-best in orange. All methods have been trained using 8 million query points. Here, we report the average and standard deviation of different performance metrics averaged over four shapes from the Stanford 3D Scanning Repository [42]; see Figure 4.

Model	CD-L1 ( $\downarrow$ )	NC ( $\uparrow$ )	NAE ( $\downarrow$ )	IoU ( $\uparrow$ )
<b>GRBFNet (Ours)</b>	<b>0.002 <math>\pm</math> 0.002</b>	<b>0.982 <math>\pm</math> 0.039</b>	<b>5.469 <math>\pm</math> 5.748</b>	<b>0.986 <math>\pm</math> 0.027</b>
NeuRBF	0.003 $\pm$ 0.004	0.969 $\pm$ 0.078	6.797 $\pm$ 9.648	0.969 $\pm$ 0.070
InstantNGP	0.002 $\pm$ 0.002	0.980 $\pm$ 0.047	5.420 $\pm$ 6.621	0.985 $\pm$ 0.032

TABLE 2

Quantitative evaluation of the performance of the proposed method in reconstructing and representing Signed Distance Fields. The best values are highlighted in green and the second-best in orange. All methods have been trained using 8 million query points. Here, we report the average and standard deviation of different performance metrics averaged over 12 shapes from the Stanford 3D Scanning Repository [42] and the DiLiGenT-MV dataset [43].

regresses both the geometry and the appearance information in the form of spherical harmonic coefficients. Thus, the inference time is very fast as one needs to only query once, a very shallow network composed of one input layer and one output layer.

**(3) Training.** We train the network end-to-end without any 3D supervision. Specifically, we minimize the  $\mathcal{L}_1$  loss between the RGB color estimated by the network and the groundtruth RGB value, averaged over the pixels in the batch. Also, when a foreground mask is available, we add a mask loss term to the overall loss. It is defined as the Binary Cross Entropy (BCE) between the mask value at a groundtruth pixel and the integration of the density values along the viewing direction through that pixel.

## 7 RESULTS

We evaluate the performance of the proposed framework in representing nD signals such as 3D geometry (Section 7.1), RGB images (Section 7.2), and radiance fields (Section 7.3). For each case, we compare performance against the state-of-the-art in terms of representation accuracy, training and inference times, and compactness of the representation. All of the experiments were undertaken on a single RTX 4096 GPU. All these results can be seen at high resolution from the project website: <https://grbfnet.github.io/>.

### 7.1 3D Reconstruction of Signed Distance Fields

We first evaluate the effectiveness of the proposed RBF-based neural network in representing Signed Distance Functions of 3D objects. We use 12 3D models of varying complexities, from the Stanford 3D Scanning Repository [42] and the DiLiGenT-MV dataset [43]. The latter includes polygonal meshes that are partially open, which introduces ambiguity

in the SDF estimation in some regions. This setup challenges the model’s robustness in generating a smooth and accurate SDF field.

Table 1 summarizes the performance of the proposed model and compares it to three state-of-the-art methods, namely: InstantNGP [9], NeuRBF [13], and FactorFields [14]. For this quantitative evaluation, we use four meshes from the Stanford Dataset that contain challenging surface structures. To ensure a fair comparison, we use the same number of training points across all methods.

Our method achieves the best performance in terms of the Chamfer Distance (CD-L1), Normal Consistency (NC), Normal Angular Error (NAE), and Intersection over Union (IoU). Importantly, our method remains compact, with around 3.8M parameters, compared to 5.3M for FactorFields and 6.1M for InstantNGP. Note that NeuRBF requires significantly fewer parameters (0.9M) but is the slowest in terms of training time (50 seconds on average). Our method is also very fast, achieving the fastest training time compared to the tested model (15 seconds on average). Thus, it offers both compactness, speed, and accuracy of the geometry representation, during inference, our model is capable of querying approximately 49 million 3D points per second. Table 2, which presents a comparison on 12 shapes selected from the two datasets, demonstrates that our method outperforms the state-of-the-art on all metrics except on the NAE where InstantNGP performs slightly better than the proposed method. Figure 4 shows a visual comparison between the extracted meshes from SDF values estimated by different methods, and with the ground truth mesh. We can clearly see that our method can faithfully reconstruct fine details; see for example the eyes of the angel statue of the last row. Section 1 in the Supplementary Material provides additional discussions and visual results.

### 7.2 Representation of 2D signals

We now evaluate the accuracy and efficiency of the proposed framework in representing multichannel 2D signals such as RGB images. We use three high-resolution images: **(1)** Summer Day<sup>1</sup>, **(2)** Pluto<sup>2</sup>, and **(3)** Girl With a Pearl Earring<sup>3</sup>. These are very complex images where the total number of pixels per image ranges from 4M to 213M. We use **(1)** the Peak Signal-to-Noise Ratio (PSNR) to measure the reconstruction quality and **(2)** the number of parameters,

1. Credit to Johan Hendrik Weissenbruch and Rijksmuseum

2. Credit to NASA

3. By Koorosh Orooj (CC BY-SA 4.0)

Method	Batch		Synthetic-NeRF			Tanks&Temples		
	size	Steps	Tr. time ↓	Size (MB) ↓	PSNR ↑	SSIM ↑	PSNR ↑	SSIM ↑
NeRF [5]	4096	300k	~35h	1.25	31.01	0.947	25.78	0.864
DVGO [6]	5000	30k	15.0m	153.0	31.95	0.957	28.41	0.911
Instant-NGP [9]	10-85k	30k	03.9m	11.64	32.59	0.960	27.09	0.905
NeuRBF [13]	4096	30k	33.6m	17.74	34.62	0.975	-	-
DiF-Grid [38]	4096	30K	12.2m	05.10	33.14	0.961	29.00	0.938
<b>Gaussian RBF-SH (Ours)</b>	4096	30K	14.3m	20.10	32.82	0.960	28.54	0.921

TABLE 3

Neural Radiance Field reconstruction. We quantitatively compare the performance of the proposed models against different NeRF methods on Synthetic-NeRF [5] and Tanks and Temples [44] datasets. The first, second, and third best values in each column are highlighted in green, orange, and yellow, respectively. "Tr. time" refers to training time.

training and inference times to measure the efficiency of the model.

In Figure 5, we show the reconstructed images using our method (top row), the PSNR as a function of the number of trainable parameters (the higher the PSNR the better), and the training time as a function of the number of trainable parameters (the lower the training time the better). We compare these metrics against InstantNGP [9] and FactorFields [38], which are state-of-the-art neural representations that support image regression. All the models were trained for 10K epochs using a batch size of  $2^{17}$  pixels randomly sampled from the image. From these figures, we observe that

- The reconstruction quality of our method, as measured by the PSNR, outperforms existing methods on the three images tested, except FactorFields whose PSNR is slightly higher than our method on two images.
- On average (from Figure 5 in the Supplementary Material), with the same number of parameters (around 29M), our method is around 12 seconds faster to train than FactorFields with only 1dB drop in reconstruction quality compared to FactorFields.
- NeuRBF and InstantNGP are faster to train but have lower PSNR.
- While InstantNGP stands out as the fastest model to train, benefiting from its highly optimized CUDA kernels, it uses a two-layer MLP decoder while ours uses only one layer.
- The proposed model strikes a balance between reconstruction performance and training efficiency as it uses only a single RBF layer operating on the feature space. Thus, it is highly parallelizable and computationally more efficient.

Finally, Section 2 in the Supplementary Material provides additional analysis, results, and discussion.

### 7.3 Radiance fields

Finally, we evaluate the performance of the proposed framework on novel view synthesis using the synthetic NeRF dataset [5] and the real Tanks and Temples dataset [44]. Table 3 quantitatively compares, in terms of training time, model size, and novel view rendering metrics, our proposed model Gaussian RBF-SH against the baseline NeRF [5] and

the latest state-of-the-art methods such as DVGO [6], InstantNGP [9], NeuRBF [13], and FactorFields [38]. In terms of training time, InstantNGP remains the fastest one since it uses its own CUDA framework for fast reconstruction. Our method, on the other hand, which uses the standard PyTorch framework and thus easily extendable to other tasks, requires, on average, 14.3 minutes to train, which is similar to FactorFields and DVGO but significantly faster than NeuRBF and the baseline NeRF. In terms of reconstruction quality, the proposed framework outperforms the state-of-the-art on the real Tanks and Temples datasets, with the exception of FactorFields whose performance is slightly better than ours. Our performance on the synthetic NeRF dataset is in line with InstantNGP but significantly outperforms the baseline NeRF, DVGO, and Plenoxels. Section 3 in the Supplementary Material provide visual comparisons of novel views generated using the proposed approach compared to the state-of-the-art. Figure 6 presents a visual comparison of rendered novel views using our model and DiF-Grid (FactorFields) [38] model. In the Chair example (first column), our model successfully captures the green reflection of the chair’s color on the decorative pattern (top row, bottom-left zoom), which is not achieved by other methods. In the Lego example (second column), our model demonstrates superior color fidelity, accurately reflecting the light’s color (see the top-right zoom). The third column highlights that our model recovers detailed rooftop patterns and even captures the stick with high accuracy. Finally, in the last column, our model accurately captures both the text and the shape. Overall, our model effectively captures fine details that FactorFields misses.

## 8 CONCLUSION

We have proposed Gaussian RBFNet, a novel compact neural representation for signals. We demonstrated that a single layer of Radial Basis Functions, with Gaussian kernels, is sufficient to accurately represent complex signals such as RGB images, 3D geometry, and radiance fields. We have demonstrated that our method achieves similar accuracy to the state-of-the-arts and outperforms baseline methods, while using the same or a fewer parameters. We believe our framework is a valuable step towards more compact neural fields. In this paper, we relied on standard PyTorch implementation and have not explored acceleration techniques similar to those used in InstantNGP [9] and Plenoxels [23]. Pursuing this direction can significantly reduce the training time of our method. Also, in this paper, we have not explored the generalization of our framework to dynamic scenes and unbounded scenes, which presents a promising avenue for future research and practical applications.

## REFERENCES

- [1] Y. Strümpfer, J. Postels, R. Yang, L. V. Gool, and F. Tombari, "Implicit neural representations for image compression," in *European Conference on Computer Vision*. Springer, 2022, pp. 74–91.
- [2] H. Chen, B. He, H. Wang, Y. Ren, S. N. Lim, and A. Shrivastava, "Nerv: Neural representations for videos," *Advances in Neural Information Processing Systems*, vol. 34, pp. 21 557–21 568, 2021.
- [3] J. J. Park, P. Florence, J. Straub, R. Newcombe, and S. Lovegrove, "DeepSDF: Learning Continuous Signed Distance Functions for Shape Representation," in *IEEE CVPR*, 2019, pp. 165–174.

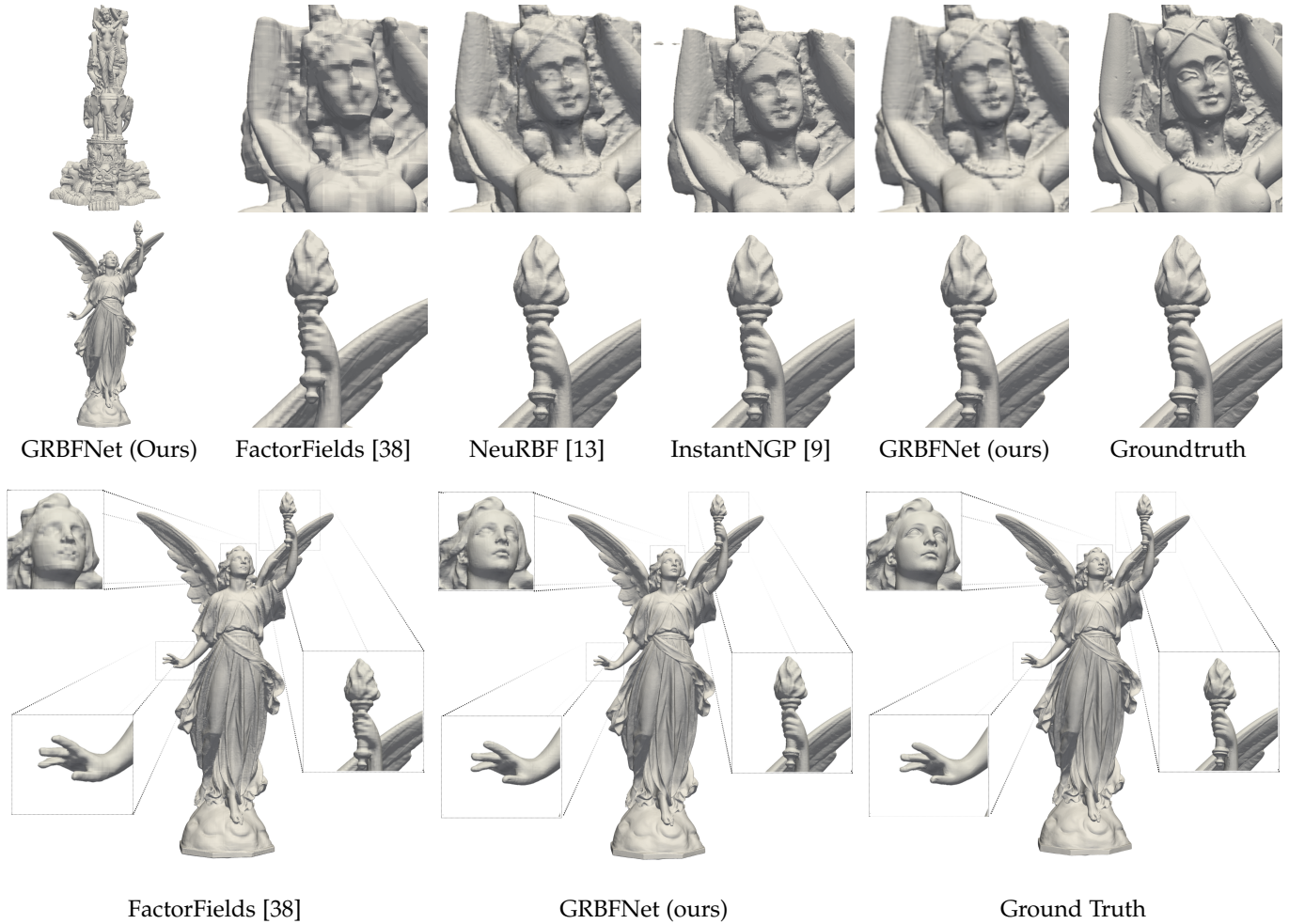


Fig. 4. Comparison of the 3D geometry reconstructed by our method against the state-of-the-art. The first column of the first two rows shows the 3D model reconstructed with our method. The remaining columns show zoomed-in views on the reconstructions obtained using state-of-the-art methods, and our method. The last column shows the groundtruth. The last row shows a zoom on some surface regions to illustrate the ability of the proposed framework to represent fine geometric details.

- [4] P. Wang, L. Liu, Y. Liu, C. Theobalt, T. Komura, and W. Wang, "NeuS: Learning neural implicit surfaces by volume rendering for multi-view reconstruction," *NeurIPS*, 2021.
- [5] B. Mildenhall, P. P. Srinivasan, M. Tancik, J. T. Barron, R. Ramamoorthi, and R. Ng, "NeRF: Representing Scenes as Neural Radiance Fields for View Synthesis," in *ECCV*. Springer, 2020, pp. 405–421.
- [6] C. Sun, M. Sun, and H.-T. Chen, "Direct voxel grid optimization: Super-fast convergence for radiance fields reconstruction," in *IEEE CVPR*, 2022, pp. 5459–5469.
- [7] S. Fridovich-Keil, A. Yu, M. Tancik, Q. Chen, B. Recht, and A. Kanazawa, "Plenoxels: Radiance fields without neural networks," in *IEEE CVPR*, 2022, pp. 5501–5510.
- [8] A. Karnewar, T. Ritschel, O. Wang, and N. Mitra, "ReLU Fields: The Little Non-linearity that Could," in *ACM SIGGRAPH*, 2022, pp. 1–9.
- [9] T. Müller, A. Evans, C. Schied, and A. Keller, "Instant Neural Graphics Primitives with a Multiresolution Hash Encoding," *ACM ToG*, vol. 41, no. 4, pp. 1–15, 2022.
- [10] B. Kerbl, G. Kopanas, T. Leimkühler, and G. Drettakis, "3d gaussian splatting for real-time radiance field rendering," *ACM Trans. Graph.*, vol. 42, no. 4, pp. 139–1, 2023.
- [11] R. Yunus, J. E. Lenssen, M. Niemeyer, Y. Liao, C. Rupprecht, C. Theobalt, G. Pons-Moll, J.-B. Huang, V. Golyanik, and E. Ilg, "Recent Trends in 3D Reconstruction of General Non-Rigid Scenes," in *Computer Graphics Forum*. Wiley Online Library, 2024, p. e15062.
- [12] G. Chen and W. Wang, "A survey on 3d gaussian splatting," *arXiv preprint arXiv:2401.03890*, 2024.
- [13] Z. Chen, Z. Li, L. Song, L. Chen, J. Yu, J. Yuan, and Y. Xu, "Neurfb: A neural fields representation with adaptive radial basis functions," *CVPR*, pp. 4182–4194, 2023.
- [14] A. Chen, Z. Xu, X. Wei, S. Tang, H. Su, and A. Geiger, "Factor fields: A unified framework for neural fields and beyond," *arXiv preprint arXiv:2302.01226*, 2023.
- [15] E. Piperakis and I. Kumazawa, "Affine transformations of 3D objects represented with neural networks," in *Proceedings Third International Conference on 3-D Digital Imaging and Modeling*. IEEE, 2001, pp. 213–223.
- [16] E. Piperakis, I. Kumazawa, and R. Piperakis, "3D object & light source representation with multi layer feed forward networks," *Neural, Parallel & Scientific Computations*, vol. 9, no. 2, pp. 161–173, 2001.
- [17] L. Liu, J. Gu, K. Zaw Lin, T.-S. Chua, and C. Theobalt, "Neural Sparse Voxel Fields," *Advances in Neural Information Processing Systems*, vol. 33, pp. 15 651–15 663, 2020.
- [18] C. Reiser, S. Peng, Y. Liao, and A. Geiger, "KiloNERF: Speeding up neural radiance fields with thousands of tiny MLPs," in *IEEE ICCV*, 2021, pp. 14 335–14 345.
- [19] T. Neff, P. Stadlbauer, M. Parger, A. Kurz, J. H. Mueller, C. R. A. Chaitanya, A. Kaplanyan, and M. Steinberger, "Donerf: Towards real-time rendering of compact neural radiance fields using depth oracle networks," in *Computer Graphics Forum*, vol. 40, no. 4. Wiley Online Library, 2021, pp. 45–59.
- [20] J. T. Barron, B. Mildenhall, D. Verbin, P. P. Srinivasan, and P. Hedman, "MiP-NeRF 360: Unbounded anti-aliased neural radiance fields," *IEEE CVPR*, pp. 5470–5479, 2022.
- [21] M. Píala and R. Clark, "Terminerf: Ray termination prediction for

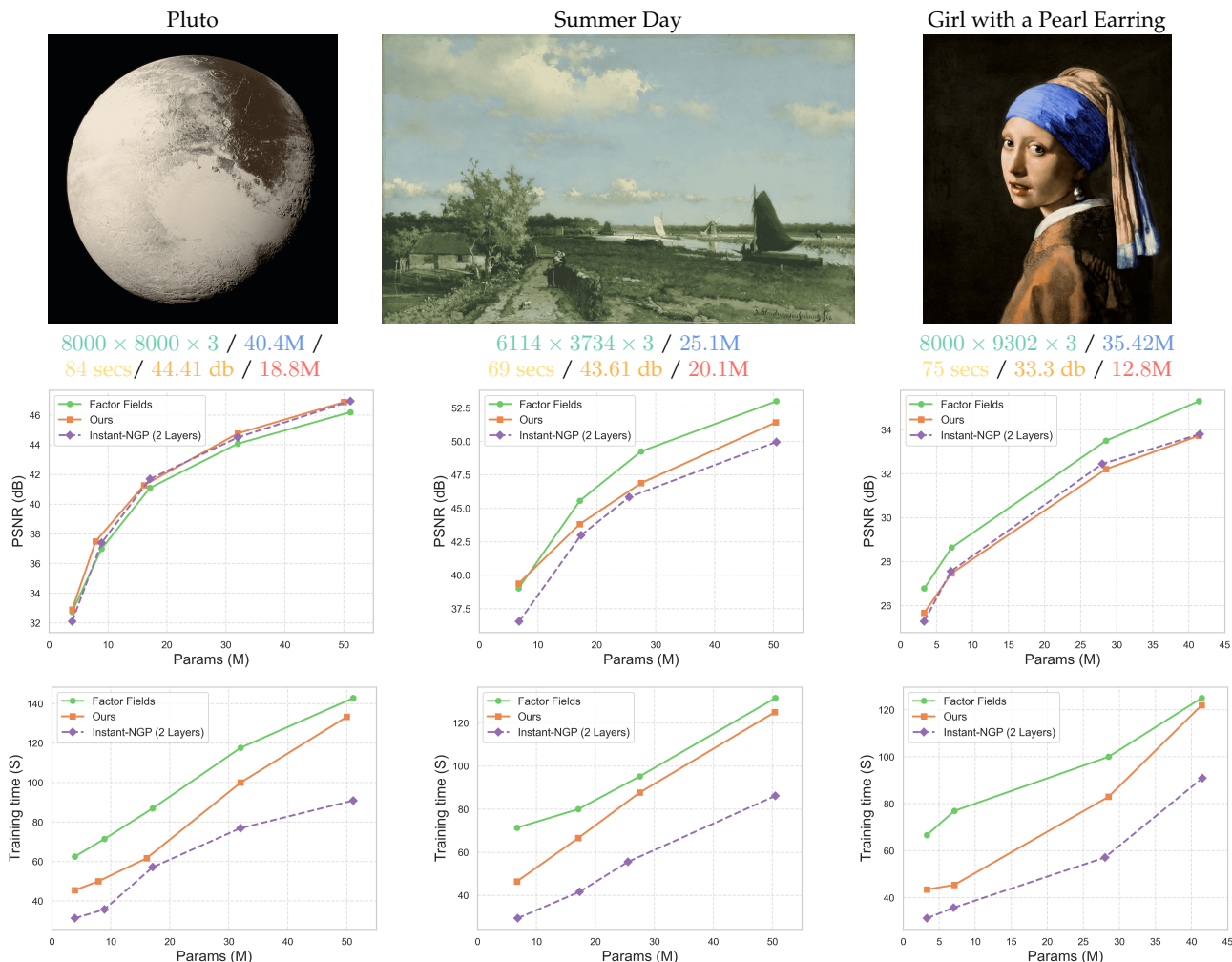


Fig. 5. Evaluation of the capacity of the proposed Gaussian RBF Network to represent 2D signals such as RGB images, compared to InstantNGP [9], and FactorFields [38]. The top row shows the images reconstructed using our method. The captions under the top row refer to the resolution of the image, the total no. of parameters of the network, the training time, the reconstruction error in terms of PSNR, and the number of pixels per sec. The model can render at runtime. The second row shows how the PSNR varies as a function of the number of parameters, while the last row shows how the training time varies as a function of the number of parameters.

- efficient neural rendering,” in *2021 International Conference on 3D Vision (3DV)*. IEEE, 2021, pp. 1106–1114.
- [22] A. Kurz, T. Neff, Z. Lv, M. Zollhöfer, and M. Steinberger, “AdaNeRF: Adaptive Sampling for Real-Time Rendering of Neural Radiance Fields,” in *ECCV*. Springer, 2022, pp. 254–270.
- [23] A. Yu, R. Li, M. Tancik, H. Li, R. Ng, and A. Kanazawa, “PleOc-trees for Real-time Rendering of Neural Radiance Fields,” in *IEEE/CVF ICCV*, 2021, pp. 5752–5761.
- [24] P. Hedman, P. P. Srinivasan, B. Mildenhall, J. T. Barron, and P. Debevec, “Baking neural radiance fields for real-time view synthesis,” in *IEEE/CVF ICCV*, 2021, pp. 5875–5884.
- [25] C. Reiser, R. Szeliski, D. Verbin, P. Srinivasan, B. Mildenhall, A. Geiger, J. Barron, and P. Hedman, “Merf: Memory-efficient radiance fields for real-time view synthesis in unbounded scenes,” *ACM Transactions on Graphics (TOG)*, vol. 42, no. 4, pp. 1–12, 2023.
- [26] L. Yariv, P. Hedman, C. Reiser, D. Verbin, P. P. Srinivasan, R. Szeliski, J. T. Barron, and B. Mildenhall, “BakedSDF: Meshing neural SDFs for real-time view synthesis,” in *ACM SIGGRAPH 2023 Conference Proceedings*, 2023, pp. 1–9.
- [27] S. J. Garbin, M. Kowalski, M. Johnson, J. Shotton, and J. Valentín, “FastNeRF: High-fidelity neural rendering at 200fps,” in *IEEE/CVF ICCV*, 2021, pp. 14346–14355.
- [28] P. Papantonakis, G. Kopanas, B. Kerbl, A. Lanvin, and G. Drettakis, “Reducing the memory footprint of 3d gaussian splatting,” *Proceedings of the ACM on Computer Graphics and Interactive Techniques*, vol. 7, no. 1, pp. 1–17, 2024.
- [29] J. C. Lee, D. Rho, X. Sun, J. H. Ko, and E. Park, “Compact 3d gaussian representation for radiance field,” in *Proceedings of the IEEE/CVF Conference on Computer Vision and Pattern Recognition*, 2024, pp. 21719–21728.
- [30] Y. Chen, Q. Wu, W. Lin, M. Harandi, and J. Cai, “Hac: Hash-grid assisted context for 3d gaussian splatting compression,” Springer, pp. 422–438, 2024.
- [31] S. Niedermayr, J. Stumpfegger, and R. Westermann, “Compressed 3d gaussian splatting for accelerated novel view synthesis,” in *Proceedings of the IEEE/CVF Conference on Computer Vision and Pattern Recognition*, 2024, pp. 10349–10358.
- [32] J. C. Carr, R. K. Beatson, J. B. Cherrie, T. J. Mitchell, W. R. Fright, B. C. McCallum, and T. R. Evans, “Reconstruction and representation of 3d objects with radial basis functions,” *Proceedings of the 28th annual conference on Computer graphics and interactive techniques*, pp. 67–76, 2001.
- [33] N. Kojekine, V. Savchenko, and I. Hagiwara, “Surface reconstruction based on compactly supported radial basis functions,” in *Geometric modeling: techniques, applications, systems and tools*. Springer, 2004, pp. 217–231.
- [34] Y. Ohtake, A. Belyaev, M. Alexa, G. Turk, and H.-P. Seidel, “Multi-level partition of unity implicits,” in *Acm Siggraph 2005 Courses*, 2005, pp. 173–es.
- [35] S. Ramasinghe and S. Lucey, “Learning positional embeddings for coordinate-mlps,” *arXiv preprint arXiv:2112.11577*, 2021.
- [36] —, “Beyond periodicity: Towards a unifying framework for activations in coordinate-MLPs,” in *European Conference on Computer Vision*. Springer, 2022, pp. 142–158.

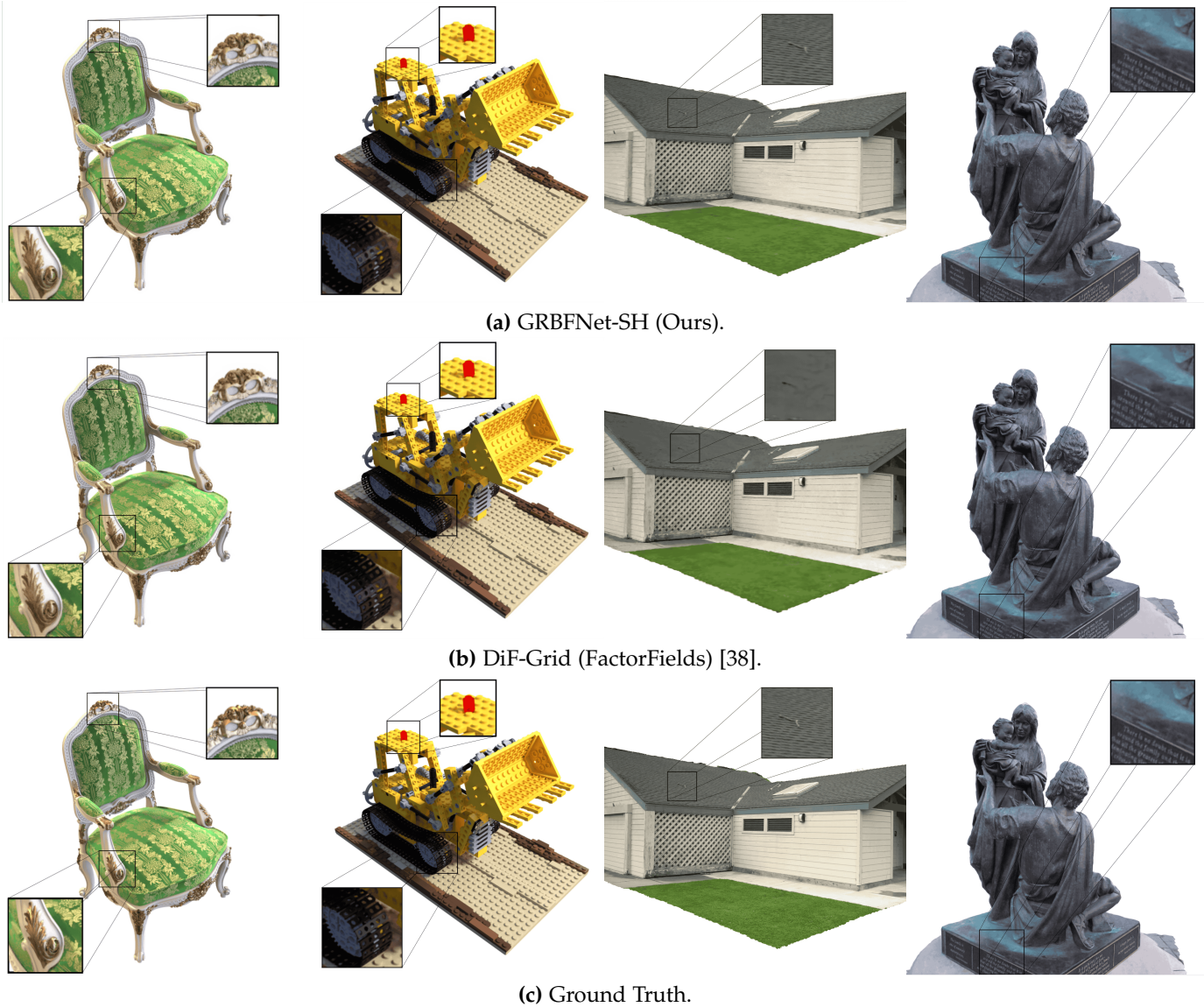


Fig. 6. Qualitative comparison of novel view generation using our model, DiF-Grid (FactorFields) model and ground truth test images. Observe in the case of the Chair, that our model is able to capture green reflection of the chair color on the decorative pattern (top row, bottom left zoom), which is not the case with other methods. The Lego example (second column) shows that our model provides better color fidelity of the reflectance on the light (see the top-right zoom). In the third column, we can see that our model is able to recover a detailed rooftop patterns. It is also able to capture the stick. Finally, the last column, is able to accurately capture the text and the shape. Overall, our model can capture small details that are missed by FactorFields.

- [37] S.-F. Chng, S. Ramasinghe, J. Sherrah, and S. Lucey, "Gaussian activated neural radiance fields for high fidelity reconstruction and pose estimation," in *European Conference on Computer Vision*. Springer, 2022, pp. 264–280.
- [38] A. Chen, Z. Xu, X. Wei, S. Tang, H. Su, and A. Geiger, "Dictionary fields: Learning a neural basis decomposition," *ACM Transactions on Graphics (TOG)*, vol. 42, no. 4, pp. 1–12, 2023.
- [39] H. Jiang, H. Yang, G. Pavlakos, and Q. Huang, "CoFie: Learning Compact Neural Surface Representations with Coordinate Fields," *NeurIPS*, 2024.
- [40] E. R. Chan, C. Z. Lin, M. A. Chan, K. Nagano, B. Pan, S. De Mello, O. Gallo, L. J. Guibas, J. Tremblay, S. Khamis *et al.*, "Efficient geometry-aware 3D generative adversarial networks," *IEEE CVPR*, pp. 16 123–16 133, 2022.
- [41] Y. Wang, I. Skorokhodov, and P. Wonka, "Pet-NeuS: Positional encoding tri-planes for neural surfaces," in *Proceedings of the IEEE/CVF Conference on Computer Vision and Pattern Recognition*, 2023, pp. 12 598–12 607.
- [42] Stanford Computer Graphics Laboratory, "Stanford 3d scanning repository," <http://graphics.stanford.edu/data/3Dscanrep/>, 1996, accessed: 2024-10-28.
- [43] M. Li, Z. Zhou, Z. Wu, B. Shi, C. Diao, and P. Tan, "Multi-view photometric stereo: A robust solution and benchmark dataset for spatially varying isotropic materials," *IEEE Transactions on Image Processing*, vol. 29, no. 1, pp. 4159–4173, 2020, [PDF available].
- [44] A. Knapitsch, J. Park, Q.-Y. Zhou, and V. Koltun, "Tanks and temples: Benchmarking large-scale scene reconstruction," *ACM Transactions on Graphics (ToG)*, vol. 36, no. 4, pp. 1–13, 2017.

# Supplementary Material: Gaussian RBFNet: Gaussian Radial Basis Functions for Fast and Accurate Neural Fields Representation and Reconstruction



In this Supplementary Material, we provide additional results and discussions that could not fit within the main manuscript. More results and source code can be accessed from the project website at: <https://grbfnet.github.io/>

## 1 3D RECONSTRUCTION OF SIGNED DISTANCE FIELDS

Algorithm 1 summarizes the entire pipeline for the SDF reconstruction process.

---

**Algorithm 1** Gaussian RBF Network for SDF Estimation

---

**Require:** Query point  $p \in \Omega$

**Require:** Multiresolution feature grid  $\mathcal{G}$

**Require:**  $N$  Gaussian basis functions with centers  $c_i$ , bandwidths  $\beta_i$ , and weights  $w_i$

**Ensure:** Estimated Signed Distance Function (SDF) value for  $p$

```

1: Feature Encoding:
2:  $\gamma(p) \leftarrow \text{InterpolateGrid}(p, \mathcal{G})$            ▷ Retrieve feature
   embedding
3:  $B \leftarrow 0$            ▷ Initialize sum of basis function outputs
4: Compute Gaussian RBF Outputs:
5: for  $i = 1$  to  $n$  do
6:    $\gamma(c_i) \leftarrow \text{InterpolateGrid}(c_i, \mathcal{G})$    ▷ Feature encoding
   of Gaussian center
7:    $d_i \leftarrow \|\gamma(p) - \gamma(c_i)\|$            ▷ Distance in feature space
8:    $\mathbf{b}_i(p) \leftarrow \exp(-\beta_i d_i^2)$            ▷ Compute Gaussian basis
   output
9:    $B \leftarrow B + w_i \mathbf{b}_i(p)$ 
10: end for
11: return  $\text{SDF}(p) \leftarrow B$ 

```

---

Figures 1, 2 and 3 show a visual comparison between the extracted meshes from SDF values estimated by different methods, and with the ground truth mesh. We can clearly see that our method can faithfully reconstruct fine details.

## 2 REPRESENTATION OF 2D SIGNALS

Figure 4 shows examples of RGB images represented using the proposed Gaussian RBFNet. In this figure, we also show

the error map. Please refer to the main manuscript for a discussion about this figure.

Figure 5 shows the PSNR score averaged over the three images as a function of the number of trainable parameters (Figure 5-(a)) and training time (Figure 5-(b)). For Figure 5-(b), the number of parameters for each method was set to match NeuRBF’s reduced number of parameters, as defined in their implementation.

Figure 6 shows how the PSNR varies as a function of the number of training epochs. This experiment confirms that our method consistently outperforms InstantNGP, NeuRBF, and, in one instance, FactorFields in terms of PSNR over extended training sessions.

## 3 RADIANCE FIELDS

Figures 7 and 8 show additional results of novel views synthesized with the proposed approach. Note that, in most of the cases, the quality of synthesized images, measured in terms of PSNR, is better or similar to the state-of-the-art.

## REFERENCES

- [1] A. Chen, Z. Xu, X. Wei, S. Tang, H. Su, and A. Geiger, “Dictionary fields: Learning a neural basis decomposition,” *ACM Transactions on Graphics (TOG)*, vol. 42, no. 4, pp. 1–12, 2023.
- [2] Z. Chen, Z. Li, L. Song, L. Chen, J. Yu, J. Yuan, and Y. Xu, “Neurfbf: A neural fields representation with adaptive radial basis functions,” *CVPR*, pp. 4182–4194, 2023.
- [3] T. Müller, A. Evans, C. Schied, and A. Keller, “Instant Neural Graphics Primitives with a Multiresolution Hash Encoding,” *ACM ToG*, vol. 41, no. 4, pp. 1–15, 2022.

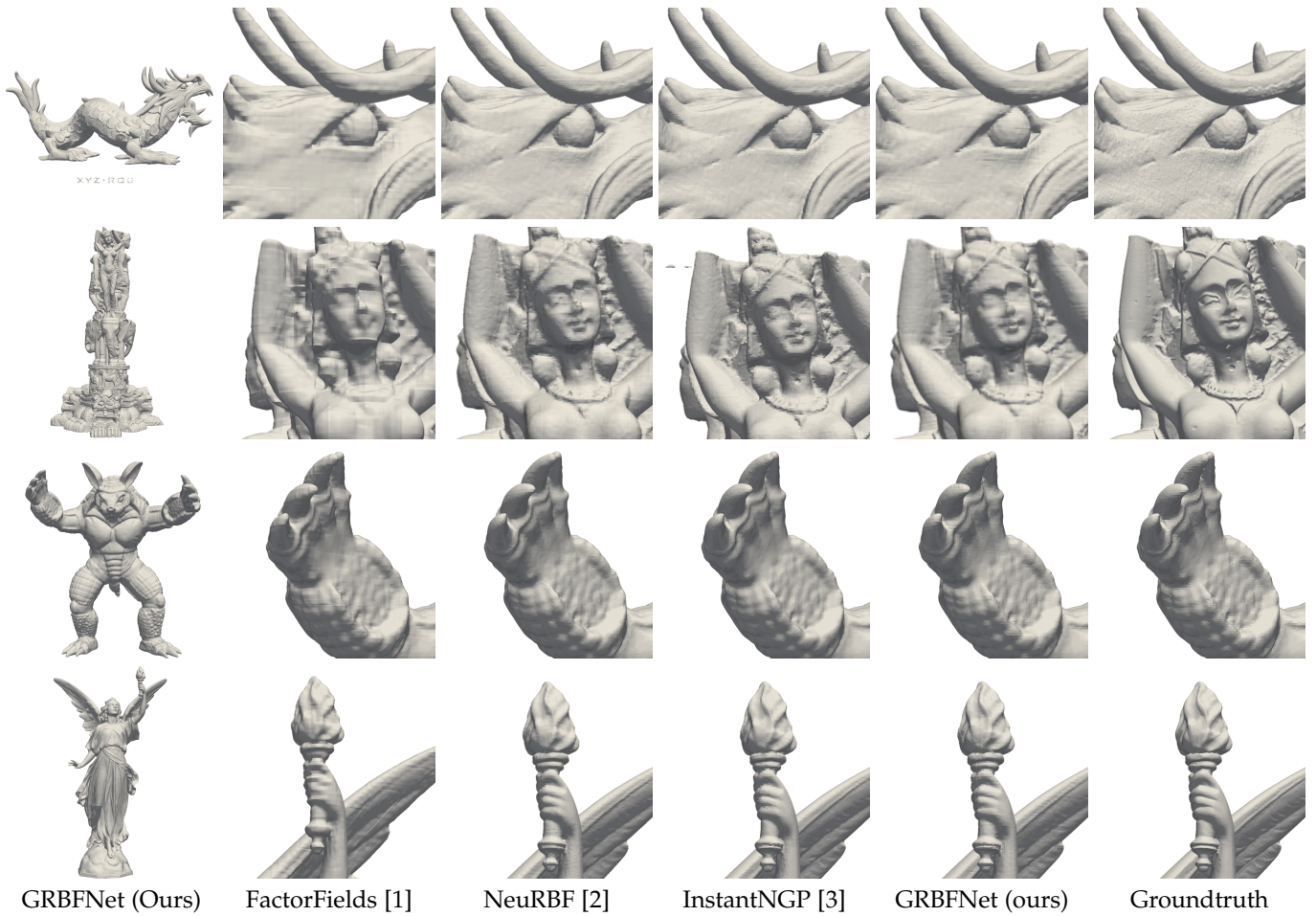


Fig. 1. Comparison of the 3D geometry reconstructed by our method and three state-of-the-art methods. The first column shows the full 3D model reconstructed with our method. The remaining columns show zoomed-in views on the reconstructions obtained using FactorFields [1], NeuRBF [2], InstantNGP [3], and our method. The last column shows the groundtruth.



Fig. 2. Qualitative comparison of the SDF reconstruction quality of our method against NeuRBF [2], InstantNGP [3], and the groundtruth.

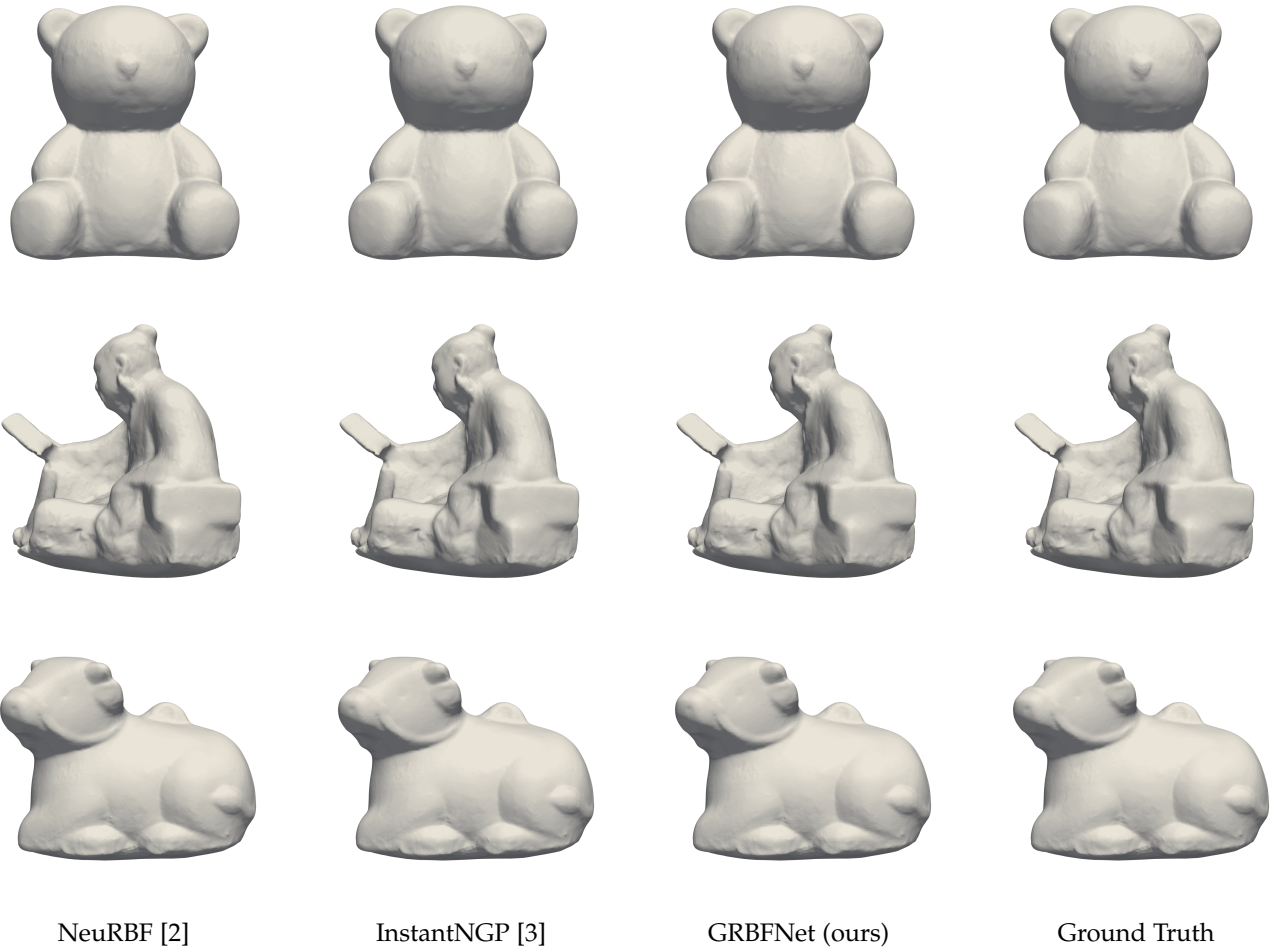


Fig. 3. Qualitative comparison of the SDF reconstruction quality of our method against NeuRBF [2], InstantNGP [3], and the groundtruth.

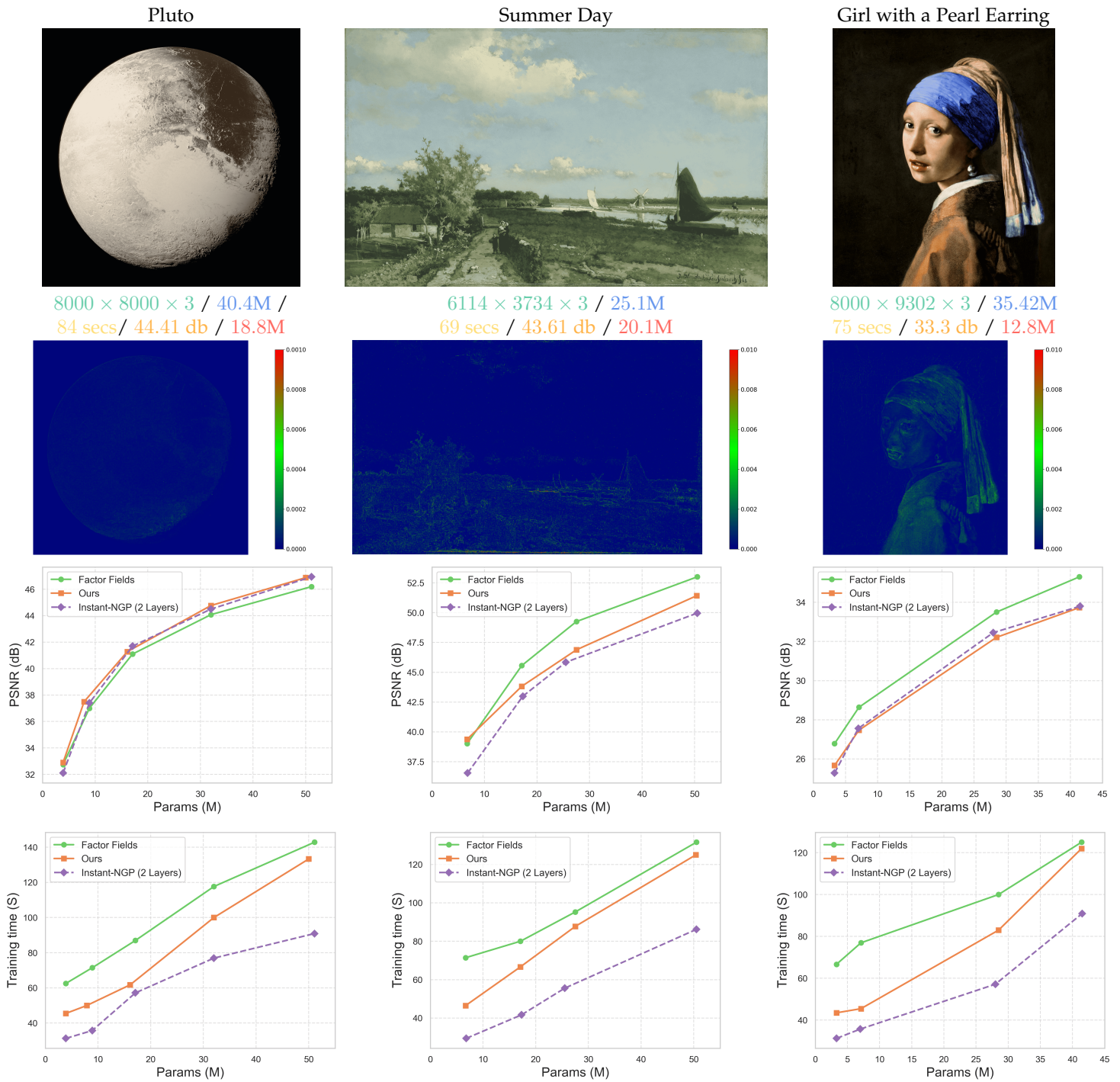


Fig. 4. Evaluation of the capacity of the proposed Gaussian RBF Network to represent 2D signals such as RGB images, compared to InstantNGP [3], and FactorFields [1]. The top row shows the images reconstructed using our method. The captions under the top row refer to the resolution of the image, the total no. of parameters of the network, the training time, the reconstruction error in terms of PSNR, and the number of pixels per sec. the model can render at runtime. The second row shows the error maps between our model regressed images and ground truth images. the third row shows how the PSNR varies as a function of the number of parameters, while the last row shows how the training time varies as a function of the number of parameters.

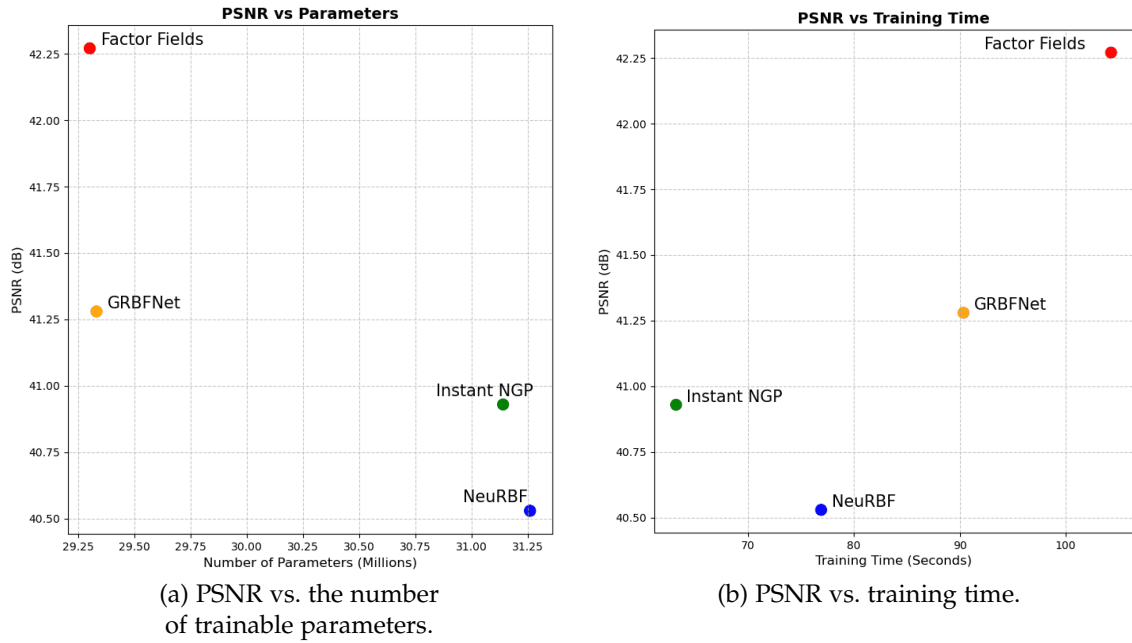


Fig. 5. Comparison of the (a) PSNR to number of trainable parameters, and (b) PSNR to training time of our model (GRBFNet) against InstantNGP [3], NeuRBF [2], and FactorFields [1].

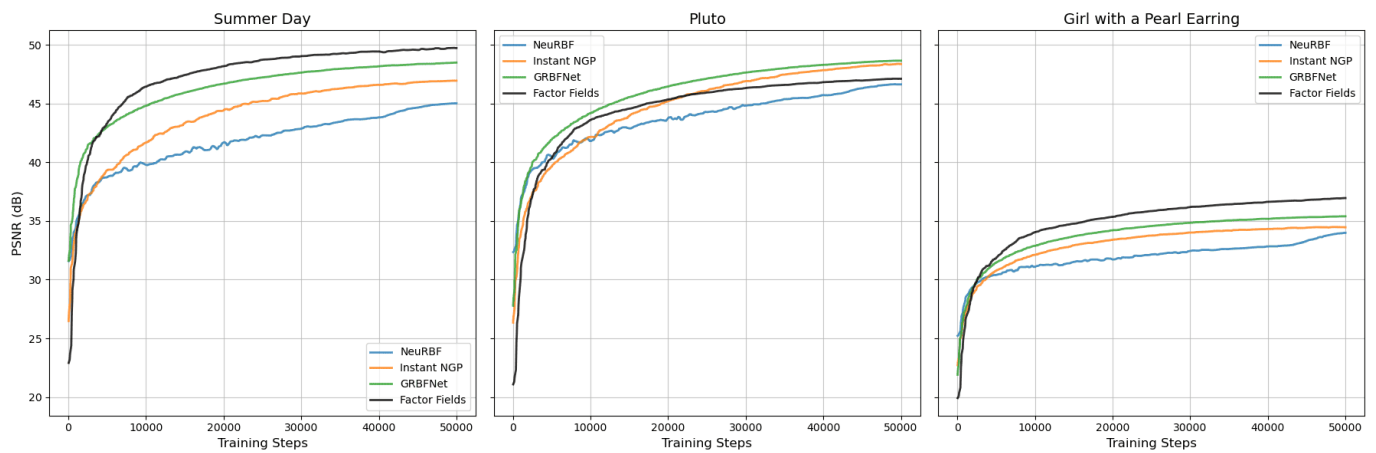


Fig. 6. Comparison of the representation accuracy of different methods in terms of PSNR as a function of the number of training epochs.



PSNR: 38.08 db  
Avg PSNR: 37.05 db



PSNR: 38.10 db  
Avg PSNR: 37.22 db



PSNR: 31.83 db  
Avg PSNR: 30.25 db



PSNR: 37.45 db  
Avg PSNR: 36.73 db

**(a) DiF-Grid (FactorFields) [1]**



PSNR: 28.50db  
Avg PSNR: 25.76 db



PSNR: 27.90db  
Avg PSNR: 25.70db



PSNR: 32.50 db  
Avg PSNR: 29.90db



PSNR: 37.92db  
Avg PSNR: 36.83 db

**(b) GRBFNet-SH (Ours)**



**(c) Ground truth**

Fig. 7. Qualitative comparison of novel view generation using our model, DiF-Grid (FactorFields) model, and ground truth test image. For each example, we show the PSNR value of the generated view and the average PSNR value over the 200 test images of the scene.



PSNR: 25.86 db  
Avg PSNR: 26.40 db



PSNR: 28.76 db  
Avg PSNR: 27.43 db



PSNR: 27.65 db  
Avg PSNR: 27.55 db

**(a) DiF-Grid (FactorFields) [1]**



PSNR: 25.69 db  
Avg PSNR: /25.82 db



PSNR: 28.84 db  
Avg PSNR: 27.38 db



PSNR: 26.90 db  
Avg PSNR: /27.92 db

**(b) GRBFNet-SH (Ours)**



**(c) Ground truth**

Fig. 8. Qualitative comparison of novel view generation using our model, DiF-Grid (FactorFields) model, and ground truth test image. For each example, we show the PSNR value of the generated view and the average PSNR value over the 200 test images of the scene.